# Precise Nanoscale Surface Modification and Coating of Macroscale Objects: Open-Environment in Loco Atomic Layer Deposition on an Automobile

Moataz Bellah M. Mousa, Christopher J. Oldham, and Gregory N. Parsons*

Department of Chemical and Biomolecular Engineering, North Carolina State University, Raleigh, North Carolina 27695, United States

ⓢ *Supporting Information*
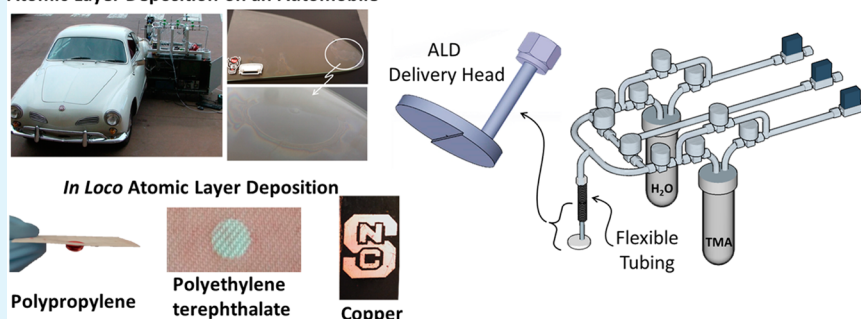
ABSTRACT: The fundamental chemical reaction conditions that define atomic layer deposition (ALD) can be achieved in an open environment on a macroscale surface too large and complex for typical laboratory reactor-based ALD. We describe the concept of in loco ALD using conventional modulated reactant flow through a surface-mounted "ALD delivery head" to form a precise nanoscale Al_2O_3 film on the window of a parked automobile. Analysis confirms that the processes eliminated ambient water contamination and met other conditions that define ALD growth. Using this tool, we demonstrate open-ambient patterned deposition, metal corrosion protection, and polymer surface modification.

KEYWORDS: atomic layer deposition, in loco, open-environment ALD, metal oxides, ALD delivery head

The basic principle of atomic layer deposition (ALD) involves a set of thermodynamically favorable self-limiting surface reactions that enable the formation of uniform and highly conformal nanoscale metal, metal oxide, and organic thin films with near-monolayer precision over large surface areas.[1−5] This self-limiting reaction scheme ensures complete surface coverage with minimal pinhole density. While the primary commercial use for ALD is in advanced electronics, ALD is also used to modify gas diffusion barriers and membranes,[6,7] passivate surfaces from corrosion and wear,[8−10] and add mechanical strength to polymers, fibers, glass, and nanostructures.[11−15] Recent advances in ALD and related molecular layer deposition also show promise for the stepwise surface synthesis of polypeptides,[16] integrated nanobatteries,[17] passivation and stabilization of molecular photoelectrochemical solar cells,[18,19] and directed modification of metal−organic framework catalysts.[20] In each ALD self-limiting growth cycle, the substrate receives a saturating dose of each reactant (typically a metal−organic and a reductant for metal, or an oxidant for metal oxide) separated in time or physical location[21−25] by inert gas. The earliest patent literature on ALD shows a range of reactor designs compatible with these basic ALD requirements,[1] and many other reactor design schemes have been developed and commercialized. Reactors are known that can operate at ambient pressure in batch,[26] roll-to-roll,[22,23] and spatial ALD geometries,[21,22,24,25] where large pliable substrates are fed through an ALD growth zone. Yet, all previous batch and spatial ALD reactor designs require the object to be coated to be carried to the reactor and placed or fed into a controlled reactor volume fixed in a laboratory or other fabrication facility. This reliance on prebuilt confined ALD reactors reflects the needs of most applications to date, but the basic requirements of the ALD process can be met using other system designs that could significantly amplify the field of use for precision nanoscale coatings and surface modification chemistry afforded by ALD.

In this work, we demonstrate a novel ALD delivery-head platform that meets the basic principles of ALD without the need for a defined reactor body and show that a portable delivery head can function outside a controlled fabrication environment to create well-defined uniform nanoscale thin-film coatings on macroscale objects that are much too large and complex for any known conventional ALD reactor in use today.
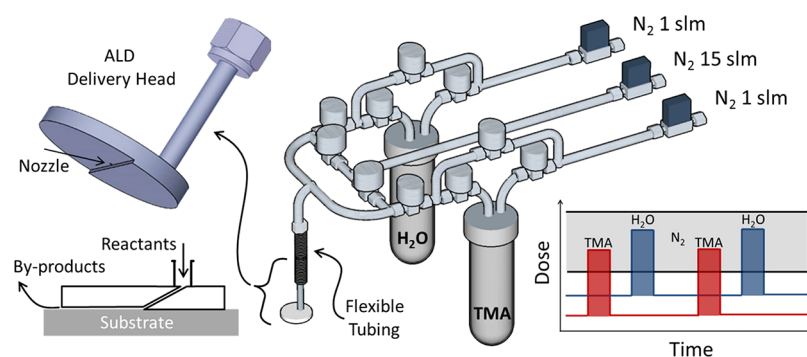
Figure 1. Reactant delivery apparatus, ALD delivery head, and gas-flow schematic for in loco ALD. The system uses sequential dosing of reactants (e.g., TMA and H_2O) separated by inert gas purge (N_2) to deposit Al_2O_3. Dry N_2 flows at up to 15 slm through a central $^1/_4$-in. delivery line. Electronic valves allow N_2 at a maximum flow of ~1 slm to intermittently flow into reactant bubblers to deliver vapors in the sequence shown. The disk-shaped ALD delivery head with a ~140 μm step milled over half the surface sits flat on the object to be coated. Gas exits through the central 1 mm nozzle and flows radially through the gap between the head and the substrate, thereby creating a semicircular ALD growth zone.
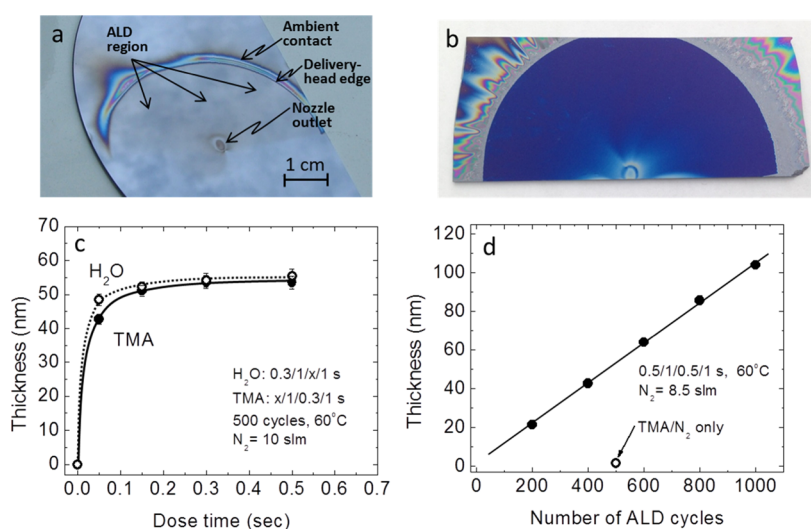
Figure 2. Results confirming well-defined ALD using the ALD delivery head. Photographs of silicon substrates coated with (a) 150 and (b) 800 $TMA/N_2/H_2O/N_2$ cycles at 60 °C, yielding uniform ALD coatings approximately 15 and 86 nm thick, respectively, in the semicircular ALD region under the delivery head, between the reactant gas entrance point and the head outer edge. Some excess coating appears at the nozzle outlet and outside the coating head, where excess TMA contacts ambient air and water to create a CVD zone. Changing the TMA and water dose times (c) and number of ALD cycles (d) leads to increasing growth saturation and linear thickness with the number of ALD cycles (~1.05 Å/cycle). A point in panel d shows that using 500 TMA/N_2 cycles with no water doses leads to less than 1 nm of film deposition, demonstrating negligible diffusion of ambient moisture to the deposition zone.

We believe that ALD coatings on macroscale objects could be used, for example, to avoid or repair damage from mechanical wear or chemical corrosion,[9,10] passivate surface scratches or defects to keep them from expanding and propagating,[12] or add UV resistance or other optical modification. Using the ALD delivery head, we show feasibility for in loco ALD by adding a precise nanocoating to the attached window of an automobile parked outdoors adjacent to our laboratory building. Film thickness measurements confirm that the tool and process met the key ALD requirements for surface saturation and linear growth per cycle without undesired side reactions. We show that the tool can create corrosion protection layers by coating copper sheets, and we extend the tool to modify the surfaces of polymer fibers and fabrics, yielding localized and controlled changes in surface wetting.[27]

The gas-flow setup and delivery-head schematic are shown in Figure 1. The reactants (trimethylaluminum, TMA, and deionized water vapor) flowed separately in a typical ALD scheme (e.g., $TMA/N_2/H_2O/N_2$) to the gas delivery head

through $^1/_4$-in. stainless steel lines connected to a flexible stainless steel bellows line. The bellows line allows the delivery head to be adjusted and configured to attach to any surface close to the system. The bottom of the 4.5-cm-diameter delivery head was milled by 140 ± 10 μm across half of the surface area, as shown in Figure 1, so that placing the head against a flat surface created a gap between the head and the surface that defines the ~8 cm² deposition zone area. The gap distance could be adjusted using spacers. The substrates for coating were typically silicon wafers with native oxide, heated to temperatures between 50 and 120 °C. The gas flows into the gap through a 1 mm nozzle inclined at 20°, designed to mimic the well-studied confined oblique impinging-jet-flow condition.[28] Previous experiments and modeling of the gas flow during low-temperature atmospheric-pressure ALD[26] show that slow species diffusion at high pressure requires longer purge periods to clear products from the growth zone, slowing the overall process throughput. The ALD delivery head shown in Figure 1 produces high gas velocities in the growth zone, which

decreases the surface boundary layer thickness and promotes fast species transport of the substrate's surface. The flow condition also avoids moisture contamination by eliminating ambient water diffusion or convective flow into the deposition region.

A typical sequence for the $TMA/N_2/H_2O/N_2$ dose times was 0.2/1/0.2/1 s, respectively, carried by the inert gas flowing at ∼10 standard liters per minute (slm), leading to good ALD over ∼8 cm^2 with a total cycle time at or near 2 s, for an overall Al_2O_3 growth rate of >3 nm/min. All experiments in the laboratory were performed in an enclosed exhaust hood. Using saturating exposures, some excess TMA exited the gap region, but it was rapidly consumed within a few millimeters of the head, posing no significant risk.

In addition to the ALD coating head design shown in Figure 1, earlier designs using a central gas entrance point and planar 360° radial flow were constructed and tested, as shown in Figure S1. For the radial-flow designs, the symmetric flow created a Bernoulli force that could hold small substrates in place over a fixed distance from the planar head. Modeling results showed laminar and turbulent regions within this gap, resulting in regular and repeatable ring patterns corresponding to ALD and chemical vapor deposition (CVD) regimes observable on the silicon substrate, and are shown in Figure S2. The delivery-head design in Figure 1 produced more uniform ALD, so it was preferred for subsequent evaluation.

Figure 2 shows the results from the open-ambient ALD delivery head on silicon wafers. The photographs in Figure 2a,b show the resulting shape and surface area of the ALD-coated region. The ALD coating is semicircular with excess nonuniform coating at the edge of the delivery head, where unused reactant (TMA) exits the growth zone and reacts with ambient ,moisture. We find that the extent of this excess growth can be controlled by the gas dose time (as discussed below), but for our studies, we use this excess growth to visibly help to locate the ALD growth region. Some excess growth is also seen at the gas inlet point, also discussed further below.

The sample in Figure 2a received 150 ALD cycles at ∼50 °C using $TMA/N_2/H_2O/N_2$ dose times =0.2/2/0.1/2 s. Using ellipsometry at more than 10 locations under the delivery head (within 1 mm from the ambient contact zone and the nozzle outlet), the film thickness was 14.6 ± 0.9 nm (variation is ± one standard deviation). The refractive index was n= 1.53 ± 0.02, consistent with other ALD Al_2O_3 layers formed at low temperature.[29] Growth at 120 °C led to ∼0.11 nm/cycle and a refractive index of 1.61 ± 0.02, consistent with a more dense film. A thicker film (t = 86.3 ± 2 nm, n = 1.55 ± 0.02) deposited using 800 ALD cycles in Figure 2b shows good color uniformity in the growth region. Using 1 s N_2 purge times, we measured the saturation behavior of the TMA and water doses, and the results are shown in Figure 2c. After 500 ALD cycles, the film thickness saturates at ∼53 ± 4 nm for TMA and water exposure times exceeding ∼0.2 s. For this reactant delivery-head design, a total gas flow rate of ∼10 slm leads to an average gas residence time of ∼10 μs in the region above the growth zone. We find that the gas purge time between reactant doses needs to be larger (>0.5 s) to ensure that the reactants are effectively removed from the manifold leading up to the delivery head. In our system, the manifold design was not optimized to decrease the required cycle time. The growth thickness versus cycle number (Figure 2d) under saturation conditions shows a linear trend with a slope of 0.105 ± 0.005 nm/cycle, consistent with traditional ALD Al_2O_3 growth

conditions observed in batch and spatial reactor designs. Error bars on the data points in Figure 2d are approximately the same size as the data-point symbols.

Photographic images of samples produced using 600 ALD cycles with various gap spacing and gas flow rates are shown in Figure 3a, demonstrating that nonoptimized conditions led to
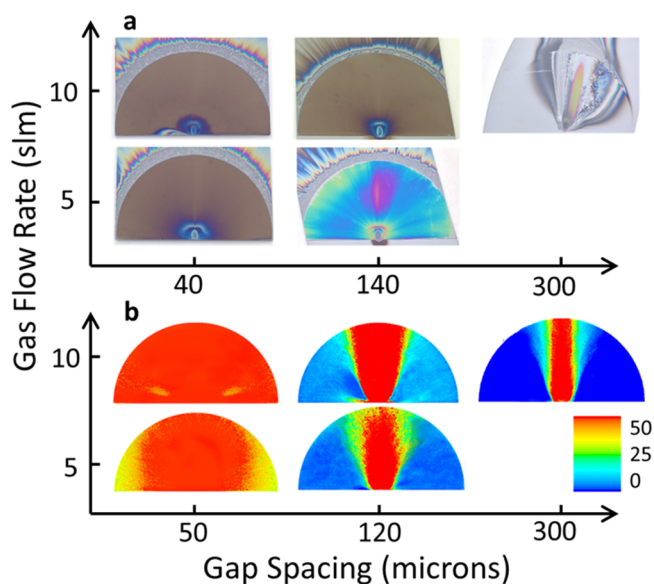
Figure 3. (a) Images for films deposited on silicon using different gap spacing and nitrogen gas flow rates. (b) Velocity contours (m/s) from CFD modeling of steady-state N_2 flow through the deposition zone at relevant conditions. Using a sufficient gas flow rate, uniform radial flow is obtained for relatively small gap sizes, leading to uniform deposition. For larger gap sizes, gas can flow straight from the nozzle through the gap. The flow gradient creates a Bernoulli force that can pull ambient air and water vapor into the growth zone, leading to visible nonuniformity in the corresponding experimental deposition images.

visible nonuniform film thickness patterns in the growth zone. To understand the observed trends, computational fluid dynamics (CFD) was used to model the gas flow in the growth zone, and model results are shown in Figure 3b, where the dark-blue regions represent areas where the gas velocity is low and the dark-red regions represent areas of high gas velocity. The model shows that thinner gap spacing and higher gas flow rate improve the gas-flow uniformity. Using a 50 μm gap with 10 slm N_2 flow, the model shows the gas-flow velocity in most of the gap ranging from 45 to 55 m/s, corresponding to viscous flow with a Reynolds number of 105−130. The sample photographs in Figure 3a generally confirm the trend predicted by the model. Using a relatively large gap size, the reactant delivery nozzle pushes the gas in a direction colinear with the gas entrance port (i.e., upward direction in Figure 3), decreasing the flow in the radial direction and leading to nonuniform growth. The model also shows that, under severe conditions, the flow-rate variation within the gap can create a pressure gradient that pulls ambient air and water vapor into the growth zone, promoting nonuniform CVD. The experiment using a ∼300 μm gap shows white particles in the growth zone, ascribed to homogeneous reaction between TMA and ambient moisture, confirming the model prediction. We also find that, under some conditions, uniformity can also be promoted by increasing the purge time between the reactant exposures. Excess growth is observed at the gas inlet point. Results from
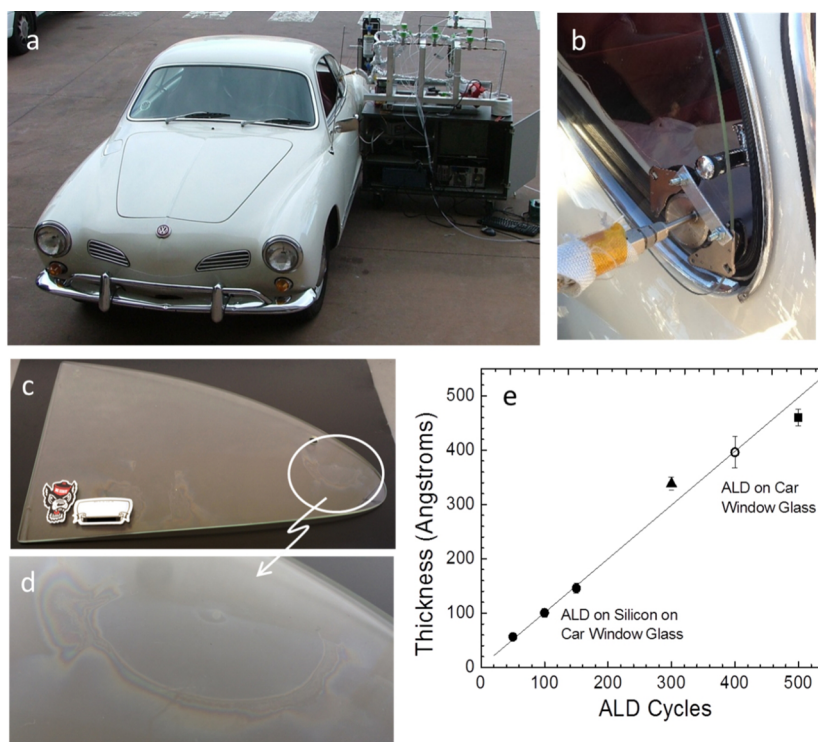
Figure 4. (a) In loco ALD apparatus adjacent to a Volkswagen automobile. (b) Close-up image of the ALD head affixed to the rear side window glass, delivering 400 cycles of ALD coating to a local region on the window at 50 °C. (c) ALD-coated window removed from the car for ellipsometry analysis. The circled region corresponds to the ALD head mounting location. (d) Close-up image showing the semicircular ALD zone outlined by multicolored CVD growth. (e) Thickness versus number of ALD cycles measured by ellipsometry for ALD coatings on silicon fixed to the car window and on the window itself. The growth per cycle of the in loco ALD tool was 0.95−1.05 Å/cycle, corresponding to a high growth rate of ∼3 nm/min.

CFD modeling show that the high gas velocity, sudden gas expansion, and change in the flow direction increase the turbulent kinetic energy near the inlet, leading to gas entrainment and CVD film growth. Consistent with flow modeling, the experimental results in Figure S4 show that the extent of CVD near the inlet can be minimized by controlling the gas purge time per cycle. Generally, the model and experimental trends show that the ALD delivery-head flow design used here performs well under controlled viscous flow, enabling uniform ALD in the growth area.

The overall motive of this work is to demonstrate that controllable nanoscale thin-film coatings can be achieved on macroscale objects, without the constraint of a reactor chamber in a well-controlled laboratory environment. Therefore, as a proof-of-concept demonstration, we transported the system shown in Figure 1 outside the laboratory and attached the ALD delivery head to the window of an automobile in a parking area adjacent to our laboratory building. This same system was used to deposit the films shown and analyzed in Figure 2. Figure 4a shows a photograph of the system on a laboratory cart, where the delivery head is attached to the automobile window, as shown in Figure 4b. In this demonstration, we chose to deposit a film on the window of an older Volkswagen because the window could be readily removed and carried to the laboratory for ellipsometry analysis.

While a variety of head-mounting approaches could be developed, we held the head in place using a neodymium magnet mounting assembly, as shown in Figure 4b. A solid bar attached to two magnets was positioned over the substrate-contacting area of the delivery head. Two additional magnets

positioned on the inside of window then squeezed the delivery head securely against the glass, reproducibly fixing the head−substrate gap distance. For the geometry in Figure 4b, gas flow is downward, producing a coating in the area under the lower half of the disk.

For the initial experiments, we attached a silicon wafer piece to the automobile window using double-sided tape and then positioned the ALD delivery head on top of the silicon wafer piece. At the start of the tests, the outdoor temperature was approximately 5 °C, warming up to 10 °C during the morning. Before a run was initiated, heated N_2 was set to flow through the mounted delivery head for about 1−2 min, raising the temperature in the growth zone to 40−50 °C, as measured by a thermocouple fixed on the inside of the window. Although not specifically studied, flowing hotter N_2 could have produced a higher window glass temperature. For the first few test runs, cold spots in the gas delivery lines led to precursor condensation, resulting in no measurable film growth. After adjustment of the line heating, coating was done using 50, 100, and 150 ALD cycles on silicon, and ellipsometry confirmed that the film thickness increased linearly with the ALD cycles. We then attached the delivery head directly to the automobile window and performed 400 ALD cycles. The window was removed from the car (Figure 4c), and using ellipsometry in 10 locations across the coated region (circled in Figure 4c and shown in Figure 4d), the thickness measured on the car window was 396 ± 12 Å. The 12 Å represents the range deviation of measured thickness from the mean of the 10 measured values. Results collected in Figure 4e show that the

film thickness scales linearly with the number of ALD cycles with a slope of 1.0 ± 0.05 Å/cycle.

As discussed above, excess reactant exiting the growth zone creates a visible multicolored CVD region, and this region is visible in the photograph of the glass window in Figure 4d, under the semicircular ALD zone. Close examination of Figure 4c reveals similar color patterns toward the bottom-middle of the window, adjacent to the locations where the silicon wafers were fixed during those tests. CVD helps us to visually identify the ALD growth zone, but it is desirable to control or eliminate the extent of this CVD growth. Under the conditions used, the 0.1 s TMA dose delivers $>1 \times 10^{17}$ TMA molecules into the growth zone. This is more than 10 times larger than the number of molecules needed to achieve saturated coverage on the ~ 16 cm^2 surface area of the substrate and the delivery-head face (see the Supporting Information). Therefore, increasing the TMA dose time enlarges the CVD region (Figure S5) and indicates that the extent of CVD can be controlled by the reactor and process design. The CVD growth on the substrate can also be eliminated using a physical mask as discussed below.

Other applications for open-air in loco ALD can also be imagined. Parts a−d of Figure 5 display examples for corrosion protection and visible pattern design on planar surfaces. It shows photographs of a clean copper plate and the copper plate after it was covered by a patterned Kapton polymer tape mask
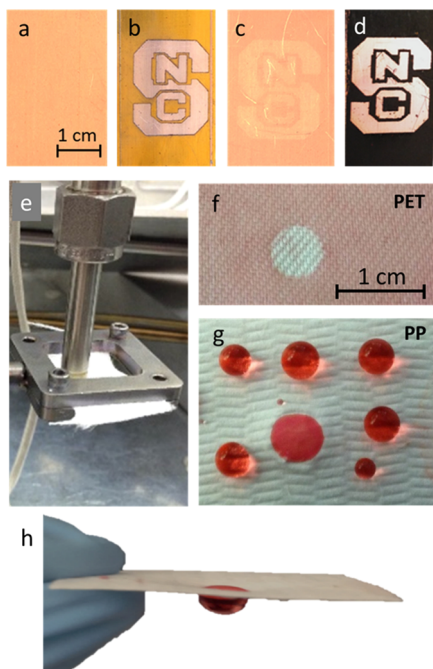
Figure 5. Example applications of in loco ALD: (a−d) corrosion protection of copper and (e−h) localized surface modification of fibers and textiles. (a) An untreated copper sheet. (b) Copper coated with a patterned polymer tape layer. (c) The tape is removed after coating under the ALD delivery head (1000 cycles, TMA/N$_2$/H$_2$O/N$_2$ = 0.1/2/0.1/2 s, N$_2$ = 8.5 slm, 65 °C). (d) After oxidation in air (400 °C, 3 h), the ALD-coated region remains unoxidized, retaining its original copper color. (e) A modified delivery head was used to deposit spot coatings of ∼5 mm diameter onto porous fiber substrates. (f) After localized coating (3 cycles, TMA/N$_2$ = 200/100 s + H$_2$O 10 s), a hydrophilic PET fabric becomes hydrophobic in the coated region, repelling red-dyed liquid water. (g and h) The same in loco ALD treatment on a hydrophobic PP fiber mat creates local hydrophilic regions that collect and hold red-dyed water droplets.

(~ 60 μm thick) and coated with 1000 ALD cycles at 60 °C using the open-air ALD delivery head. The pattern on the tape mask was formed using a laser cutter and then removing the cut area to partially expose the copper substrate (i.e., within the letters "NCS", Figure 5b). Parts c and d of Figures 5 respectively show the patterned ALD coating after removal of the mask and the coated copper sample after oxidation in air at 400 °C for 3 h. The patterned ALD layer protects the coated copper regions from oxidative corrosion, creating a visible image that faithfully mimics the patterned mask and ALD metal oxide. In these tests, the polymer mask extends under the coating head base and beyond the coating head edge, Therefore, the flow gap spacing between the delivery head and the tape surface remains unchanged but increases by 60 μm (e.g., from ∼120 to 180 μm) in the region being coated. Using a purge time of 1 s after the TMA and water dose steps for 1000 ALD cycles, the nonuniform gap spacing leads to some excess growth at the edges of the mask, likely due to local reactant trapping. Using the same number of ALD cycles, increasing the purge time to 2 s/cycle eliminated the visible nonuniformity.

We further find that the in loco ALD design can be adapted to coat porous substrates such as nonwoven fiber mats and woven textiles for controlled surface wetting and localized liquid capture. The photographs in Figure 5e−g show an ALD gas-delivery tube directing reactant flow onto a fiber substrate and the results of poly(ethylene terephthalate) (PET) and polypropylene (PP) fiber samples coated locally with ALD Al$_2$O$_3$. On the native hydrophobic PP, a conformal ALD Al$_2$O$_3$ coating deposited at low temperature is known to create a relatively smooth hydrophilic surface finish.[27,30] As shown here in Figure 5h, the surface is sufficiently hydrophilic to fix and hold a water droplet when suspended. When the hydrophilic PET fibers are exposed to water (containing a red dye for visualization), the coated region becomes hydrophobic completely through the substrate thickness, likely due to surface roughening.[27,30] Such fiber patterning could be effective, for example, for low-cost microfluidics, localized biomedical absorbents, fiber material labeling, branding or personal identification, rapid microvolumetric liquid collection and separation, and other future uses.

The in loco ALD design requires sufficient gas flow through the gap region between the growth head and the substrate (or between fibers for coating of fabrics) to exclude or minimize ambient gas contamination. While beyond the scope of this work, the results and scaling trends demonstrated here suggest that design modifications could achieve in loco ALD on other surfaces, including microscopically rough and/or macroscopically nonplanar objects. For flat rough surfaces, transporting reactants through stagnant flow regions would require longer exposure times per cycle. A smooth curved surface could be coated using a small delivery head, sized to be smaller than the surface radius of curvature (see the Supporting Information). Surfaces that are both rough and curved (such as rock sculptures, engineered structures, or any abraded surface) would require more sophisticated or tailored head designs.

Overall, we show that the fundamental conditions for self-limited monolayer scale control of surface thin-film formation reactions that define ALD can be achieved in an open environment on a macroscale surface too large and complex for typical laboratory reactor-based ALD. We developed the concept of a flexible ALD delivery head and demonstrated it by coating an automobile window with ALD Al$_2$O$_3$ outside of a

well-controlled laboratory environment. Combining modeling and experiments, we defined process requirements and demonstrated surface-saturating growth and effective elimination of ambient water contamination, even in a demanding open-air outdoor environment, giving ALD growth rates of 1.0 ± 0.05 Å/cycle consistent with the laboratory ALD. The design allowed fast growth of Al_2O_3 at ~2 s/cycle or ~3 nm/min. The ALD delivery-head tool is compatible with patterned surface coating, and the resulting ALD films function similarly to typical laboratory ALD for corrosion protection and polymer surface modification. The basic ALD delivery head, gas system design, and process conditions shown here could be substantially simplified and tailored to enable in loco ALD to protect, encapsulate, repair, optically or physically modify, or otherwise improve objects of any size fixed in most any location.

■ ASSOCIATED CONTENT

ⓢ Supporting Information

The Supporting Information is available free of charge on the ACS Publications website at DOI: 10.1021/acsami.5b05262.

> More details of the experimental methods used and the model setup, as well as results from other delivery-head designs tested in this work, and discussion and data on limiting the CVD zone extent at the reactant inlet and the delivery head edge (PDF)

■ AUTHOR INFORMATION

Corresponding Author

*E-mail: gnp@ncsu.edu.

Author Contributions

The manuscript was written through contributions of all authors. All authors have given approval to the final version of the manuscript.

Notes

The authors declare no competing financial interest.

■ ACKNOWLEDGMENTS

■ REFERENCES

(1) Suntola, T. S.; Pakkala, A. J.; Lindfors, S. G. Apparatus for performing growth of compound thin films. U.S. Patent 4,389,973A, June 28, 1983.

(2) Puurunen, R. L. Surface chemistry of atomic layer deposition: A case study for the trimethylaluminum/water process. *J. Appl. Phys.* **2005**, *97* (12), 121301.

(3) Knez, M.; Nielsch, K.; Niinistö, L. Synthesis and surface engineering of complex nanostructures by atomic layer deposition. *Adv. Mater.* **2007**, *19* (21), 3425−3438.

(4) George, S. M. Atomic Layer Deposition: An Overview. *Chem. Rev.* **2010**, *110* (1), 111−131.

(5) Miikkulainen, V.; Leskelä, M.; Ritala, M.; Puurunen, R. L. Crystallinity of inorganic films grown by atomic layer deposition: Overview and general trends. *J. Appl. Phys.* **2013**, *113* (2), 021301.

(6) Dameron, A. A.; Davidson, S. D.; Burton, B. B.; Carcia, P. F.; McLean, R. S.; George, S. M. Gas Diffusion Barriers on Polymers Using Multilayers Fabricated by Al2O3 and Rapid SiO2 Atomic Layer Deposition. *J. Phys. Chem. C* **2008**, *112* (12), 4573−4580.

(7) Jiang, Y.-B.; Liu, N.; Gerung, H.; Cecchi, J. L.; Brinker, C. J. Nanometer-thick conformal pore sealing of self-assembled mesoporous silica by plasma-assisted atomic layer deposition. *J. Am. Chem. Soc.* **2006**, *128* (34), 11018−11019.

(8) Mayer, T. M.; Elam, J. W.; George, S. M.; Kotula, P. G.; Goeke, R. S. Atomic-layer deposition of wear-resistant coatings for microelectromechanical devices. *Appl. Phys. Lett.* **2003**, *82* (17), 2883−2885.

(9) Nistorica, C.; Liu, J.-F.; Gory, I.; Skidmore, G. D.; Mantiziba, F. M.; Gnade, B. E.; Kim, J. Tribological and wear studies of coatings fabricated by atomic layer deposition and by successive ionic layer adsorption and reaction for microelectromechanical devices. *J. Vac. Sci. Technol., A* **2005**, *23* (4), 836−840.

(10) Abdulagatov, A. I.; Yan, Y.; Cooper, J. R.; Zhang, Y.; Gibbs, Z. M.; Cavanagh, A. S.; Yang, R. G.; Lee, Y. C.; George, S. M. Al2O3 and TiO2 Atomic Layer Deposition on Copper for Water Corrosion Resistance. *ACS Appl. Mater. Interfaces* **2011**, *3* (12), 4593−4601.

(11) Lee, S.-M.; Pippel, E.; Gosele, U.; Dresbach, C.; Qin, Y.; Chandran, C. V.; Brauniger, T.; Hause, G.; Knez, M. Greatly Increased Toughness of Infiltrated Spider Silk. *Science* **2009**, *324* (5926), 488−492.

(12) Jylhae, O.; Putkonen, M.; Pakkala, A. J.; Jylha, O. Strengthened structural module used for display device comprises coating arranged conformally on glass substrate, second substrate and spacer element, on surfaces facing the outside of module for increasing strength of module. U.S. Patent2012307193-A1.

(13) Meza, L. R.; Das, S.; Greer, J. R. Strong, lightweight, and recoverable three-dimensional ceramic nanolattices. *Science* **2014**, *345* (6202), 1322−1326.

(14) Atanasov, S. E.; Oldham, C. J.; Slusarski, K. A.; Taggart-Scarff, J.; Sherman, S. A.; Senecal, K. J.; Filocamo, S. F.; McAllister, Q. P.; Wetzel, E. D.; Parsons, G. N. Improved cut-resistance of Kevlar® using controlled interface reactions during atomic layer deposition of ultrathin (< 50 A) inorganic coatings. *J. Mater. Chem. A* **2014**, *2* (41), 17371−17379.

(15) Gregorczyk, K. E.; Pickup, D. F.; Sanz, M. G.; Irakulis, I. A.; Rogero, C.; Knez, M.; Tuning. Tuning the Tensile Strength of Cellulose through Vapor Phase Metalation. *Chem. Mater.* **2015**, *27*, 181.

(16) Fu, Y.; Li, B.; Jiang, Y.-B.; Dunphy, D. R.; Tsai, A.; Tam, S.-Y.; Fan, H.; Zhang, H.; Rogers, D.; Rempe, S.; et al. Atomic Layer Deposition of L-Alanine Polypeptide. *J. Am. Chem. Soc.* **2014**, *136* (45), 15821−15824.

(17) Liu, C.; Gillette, E. I.; Chen, X.; Pearse, A. J.; Kozen, A. C.; Schroeder, M. A.; Gregorczyk, K. E.; Lee, S. B.; Rubloff, G. W. An all-in-one nanopore battery array. *Nat. Nanotechnol.* **2014**, *9* (12), 1031−1039.

(18) Hanson, K.; Losego, M. D.; Kalanyan, B.; Ashford, D. L.; Parsons, G. N.; Meyer, T. J. Stabilization of [Ru(bpy)2(4,4′-(PO3H2)bpy)]2+ on Mesoporous TiO2 with Atomic Layer Deposition of Al2O3. *Chem. Mater.* **2013**, *25* (1), 3−5.

(19) Son, H.-J.; Prasittichai, C.; Mondloch, J. E.; Luo, L.; Wu, J.; Kim, D. W.; Farha, O. K.; Hupp, J. T. Dye stabilization and enhanced photoelectrode wettability in water-based dye-sensitized solar cells through post-assembly atomic layer deposition of TiO2. *J. Am. Chem. Soc.* **2013**, *135* (31), 11529−11532.

(20) Mondloch, J. E.; Bury, W.; Fairen-Jimenez, D.; Kwon, S.; DeMarco, E. J.; Weston, M. H.; Sarjeant, A. A.; Nguyen, S. T.; Stair, P. C.; Snurr, R. Q.; et al. Vapor-Phase Metalation by Atomic Layer Deposition in a Metal−Organic Framework. *J. Am. Chem. Soc.* **2013**, *135* (28), 10294−10297.

(21) Levy, D. H.; Freeman, D.; Nelson, S. F.; Cowdery-Corvan, P. J.; Irving, L. M. Stable ZnO thin film transistors by fast open air atomic layer deposition. *Appl. Phys. Lett.* **2008**, *92* (19), 192101−192101.

(22) Poodt, P.; Cameron, D. C.; Dickey, E.; George, S. M.; Kuznetsov, V.; Parsons, G. N.; Roozeboom, F.; Sundaram, G.; Vermeer, A. Spatial atomic layer deposition: A route towards further industrialization of atomic layer deposition. *J. Vac. Sci. Technol., A* **2012**, *30* (1), 010802.

(23) Dickey, E.; Barrow, W. A. High rate roll to roll atomic layer deposition, and its application to moisture barriers on polymer films. *J. Vac. Sci. Technol., A* **2012**, *30* (2), 021502.

(24) Ellinger, C. R.; Nelson, S. F. Selective Area Spatial Atomic Layer Deposition of ZnO, Al2O3, and Aluminum-Doped ZnO Using Poly (vinyl pyrrolidone). *Chem. Mater.* **2014**, *26* (4), 1514−1522.

(25) Muñoz-Rojas, D.; MacManus-Driscoll, J. Spatial atmospheric atomic layer deposition: a new laboratory and industrial tool for low-cost photovoltaics. *Mater. Horiz.* **2014**, *1* (3), 314−320.

(26) Mousa, M. B. M.; Oldham, C. J.; Jur, J. S.; Parsons, G. N. Effect of temperature and gas velocity on growth per cycle during Al2O3 and ZnO atomic layer deposition at atmospheric pressure. *J. Vac. Sci. Technol., A* **2012**, *30* (1), 01A155.

(27) Hyde, G. K.; Scarel, G.; Spagnola, J. C.; Peng, Q.; Lee, K.; Gong, B.; Roberts, K. G.; Roth, K. M.; Hanson, C. A.; Devine, C. K.; et al. Atomic Layer Deposition and Abrupt Wetting Transitions on Nonwoven Polypropylene and Woven Cotton Fabrics. *Langmuir* **2010**, *26* (4), 2550−2558.

(28) Garimella, S. V. Heat Transfer and Flow Fields in Confined Jet Impingement. *Annu. Rev. Heat Transfer* **2000**, *11* (11), 413−494.

(29) Groner, M. D.; Fabreguette, F. H.; Elam, J. W.; George, S. M. Low-temperature Al2O3 atomic layer deposition. *Chem. Mater.* **2004**, *16* (4), 639−645.

(30) Jur, J. S.; Spagnola, J. C.; Lee, K.; Gong, B.; Peng, Q.; Parsons, G. N. Temperature-dependent subsurface growth during atomic layer deposition on polypropylene and cellulose fibers. *Langmuir* **2010**, *26* (11), 8239−8244.